



1

2

3 **A New Look into the Impacts of Dust Radiative Forcing on the**
4 **Energetics of Tropical Easterly Waves**

5

6 Farnaz E Hosseinpour^{1,2} and Eric M Wilcox¹

7

8 ¹ Desert Research Institute

9 Reno, NV 89512

10 ² University of Nevada, Reno

11 Reno, NV 89557

12

13 Corresponding author's email address: Farnaz@dri.edu

14

15 **Keywords**

16 Saharan Air Layer, dust, aerosol radiative forcing, wave activity, eddy kinetic energy,
17 tropical Atlantic Ocean, African easterly jet, African easterly waves, MERRA-2, MODIS

18

19 **Abstract**

20 Saharan dust aerosols are often embedded in tropical easterly waves, also known
21 as African easterly waves, and are transported thousands of kilometers across the tropical



1 Atlantic Oceans, reaching the Caribbean Sea, Amazon Basin, and the eastern U.S.
2 However, due to the complexity of the African and Atlantic climate dynamics, there is still
3 a lack of understanding of how dust particles may influence the development of African
4 easterly waves, which are coupled to deep convective systems over the tropical Atlantic
5 Ocean and in some cases may seed the growth of tropical cyclones. Here we apply 22 years
6 of daily satellite observations and reanalysis data to explore the relationships between dust
7 in the Saharan air layer and the development of African easterly waves. Our findings show
8 that dust aerosols are not merely transported by the African easterly jet and the African
9 easterly waves system across the tropical Atlantic Ocean, but also contribute to the changes
10 in the eddy energetics of the African easterly waves.

11 The radiative forcing efficiency of dust in the atmosphere is estimated to be a
12 warming of approximately 20 Wm^{-2} over the ocean and 35 Wm^{-2} over land. This diabatic
13 heating of dust aerosols in the Saharan Air Layer acts as an additional energy source to
14 increase the growth of the waves. The enhanced diabatic heating of dust leads to the
15 increase in meridional temperature gradients in the baroclinic zone, where eddies extract
16 available potential energy from the mean-flow and convert it to eddy kinetic energy. This
17 suggests that diabatic heating of dust aerosols can increase the eddy kinetic energy of the
18 African easterly waves and enhance the baroclinicity of the region. Our findings also show
19 that dust outbreaks over the tropical Atlantic Ocean precede the development of baroclinic
20 waves downstream of the African easterly jet, which suggests that the dust radiative forcing
21 has the capability to trigger the generation of the zonal and meridional transient eddies in
22 the system comprising the African Easterly Jet and African easterly waves.



1 **1 Introduction**

2 African Easterly Waves (AEWs), also known as tropical Atlantic easterly waves,
3 are synoptic-scale atmospheric disturbances with a preferred wavelength in the 2000-
4 4000km range that often develop into tropical Atlantic cyclones (Dunn, 1940). The basic
5 characteristics and behavior of the AEWs have been described in previous studies (Charney
6 and Stern, 1962; Chang, 1993; Kiladis et al., 2006; Diaz and Aiyyer, 2013). Local heating
7 is a dominant factor in determining the growth of AEWs over West Africa (Norquist et al.,
8 1977), such that the presence of diabatic heating near the entrance of the African Easterly
9 Jet (AEJ) is a favorable factor in generating AEWs (Thorncroft et al., 2008; Russell et al.,
10 2020). The localized mid- to lower-tropospheric heating generates vortices in the vicinity
11 of the AEJ core, which is the genesis of the AEWs (Thorncroft et al., 2008; Berry and
12 Thorncroft, 2012). AEWs can be initiated by convective triggers over the highlands of
13 eastern Africa and forcing from the subtropical Atlantic storm track (Cornforth et al. 2009).

14 Several studies have shown that AEWs are intensified in the presence of convective
15 systems where the mesoscale convection and synoptic-scale AEWs are dynamically
16 coupled (Kiladis et al., 2006; Hsieh and Cook, 2005&2007; Berry and Thorncroft, 2012).
17 A large portion of tropical Atlantic cyclones and hurricanes evolve from the AEWs (Avila
18 and Clark, 1989; Avila and Pasch, 1992; Pasch and Avila, 1994) during the boreal summer
19 seasons, which is the season when the amplitude of AEWs peaks (e.g., Roundy and Frank,
20 2004).

21 Numerous studies addressed the dynamics of the AEWs; however, the impacts of
22 aerosols radiative forcing on the energy of the AEWs are poorly understood. The Sahara
23 Desert in North Africa is the largest source of dust in the world, where over sixty million



1 tons of dust particles (e.g., Prospero and Lamb, 2003; Lau and Kim, 2007) are lifted
2 annually and transported within the Saharan Air Layer (SAL) across the Atlantic Ocean
3 (Carlson and Prospero, 1972) and reaches the Caribbean Sea, the Gulf of Mexico, Amazon
4 Basin and the United States (e.g., Perry et al., 1997; Liu et al., 2008, Francis et al., 2020).
5 Dust particles in the SAL have a robust influence on regional and global climate through
6 their impacts on radiation, clouds, hydrological cycle, and atmospheric circulation
7 (Colarco et al., 2003; Lau et al., 2009; Wilcox et al., 2010; Kim et al., 2010). In particular,
8 among aerosol species, dust is known for having a strong shortwave radiative effect by
9 both efficiently scattering, as well as absorbing, incoming radiation and leading to a heating
10 of the dust layer and strong cooling of the surface (Myhre et al., 2004; Mamun et al., 2021,
11 Francis et al., 2022). The shortwave radiative effect is slightly counteracted by the
12 longwave radiative effect of dust which causes warming at the surface and cooling within
13 the atmosphere (Meloni et al., 2018).

14 A limited number of studies have focused on the impacts of Saharan dust plumes
15 on the dynamics of the AEWs (Jones et al., 2003; Ma et al., 2012; Hosseinpour and Wilcox,
16 2014). Jones et al. (2004) suggested that dust optical and radiative properties have
17 significant impacts on the AEWs. They showed that the low-level temperature anomalies
18 associated with the AEWs are modulated by dust radiative forcing and suggested that dust
19 loading in the SAL precedes the maximum geopotential height at 700-hPa by about 1-2
20 days. Model sensitivity studies have also shown that the intensification of AEWs can be
21 induced by dust (Ma et al., 2012; Grogan et al., 2019; Bercos-Hickey and Patricola, 2021;
22 Grogan et al., 2022). The analytical and numerical study of Grogan et al. (2016) found that
23 the presence of dust enhances the development of AEWs by providing a buoyancy source.



1 They also showed that dust can affect the propagation of AEWs by changing the wind shear
2 and stability of the atmosphere. Using a regional climate model coupled with a dust model,
3 Bercos-Hickey et al. (2017) found that Saharan dust causes AEJ to shift northward,
4 upward, and westward, and this results in westward expansion and the northward shift of
5 both the northern and southern tracks of the AEWs. Satellite observations support this
6 notion by showing that a similarity exists between the pattern of temperature and wind
7 anomalies of the AEWs and those associated with the dust outbreaks (Hosseinpour and
8 Wilcox, 2014).

9 Saharan dust is not the only contributor to aerosol radiative forcing over Africa
10 and the Atlantic Ocean. Previous studies showed that smoke transport from biomass
11 burning can reach up to ~ 3-5 km altitude, which is above the stratocumulus clouds over
12 the Sahel region, and may affect the radiation through aerosol direct and indirect effects
13 (Redemann et al., 2021). Biomass burning in Africa is closely related to seasonal rainfall
14 variability and the location of the Intertropical Convergence Zone (ITCZ); thus, the
15 emissions from biomass burning in North Africa occur in boreal spring and winter, when
16 ITCZ is south of the equator (e.g., Cahoon et al., 1992; Barbosa et al., 1999; Ramo et al.,
17 2020). During the boreal winter, smoke aerosols are maximized over the Sahel region
18 (Figure 1, Haywood et al., 2008), where the northward transport of smoke merges with
19 dry southward and westward transport of dust aerosols. This leads to the co-existence of
20 dust and smoke, as smoke is dominated on the top of the dust layer (Haywood et al., 2008).
21 However, during the boreal summer, biomass burning mainly occurs in South Africa,
22 where the air circulations transport smoke plumes toward the South-East Atlantic off-
23 coasts of Namibia and Angola (Zuidema et al., 2016; Cochrane et al., 2022). To study the



1 effects of Saharan dust aerosols on AEWs with avoiding the major impact of smoke
2 transport from biomass burning in South Africa, we focus our study on the region above
3 5° N latitude in West Africa and the eastern Atlantic Ocean in boreal Summer, where the
4 contribution of aerosols from biomass burning is less than 15% by mass over this region
5 (Matsuki et al., 2010). This study focuses on boreal summer season, because during this
6 season, the amplitude of AEWs peaks (e.g., Roundy and Frank, 2004), and Saharan dust
7 storms are active with less simultaneous transport of smoke from South Africa biomass
8 burning.

9 While previous studies showed the impacts of dust aerosols on climate (Ming and
10 Ramaswamy, 2011; Hosseinpour and Wilcox, 2014; Chen et al., 2021; Liang et al., 2021;
11 Grogan et al., 2022), hydrological cycle (Konare et al., 2005; Kim et al., 2010; Bercos-
12 Hickey et al., 2020) and cloud properties (Weinzierl et al., 2017; Haarig et al., 2019),
13 these elements of the climate system in this region exhibit strong variability due to AEWs.
14 To understand the details of interactions between dust aerosols and climate over the
15 Atlantic Ocean, it is essential to understand how the evolution of AEWs is determined by
16 both diabatic heating, as well as exchanges of eddy kinetic energy (EKE) within the jet-
17 wave system and how dust may contribute to the energy driving AEWs. Toward this goal,
18 we apply eddy energetic concepts to further analyze the relationships between dust and
19 the AEJ-AEWs system to gain insight into the impacts of dust aerosol radiative forcing
20 on the development of AEWs and the distribution of kinetic energy from the source of
21 instability (i.e., AEJ). Section 2 summarizes the data and methodology. Section 3
22 discusses the summary of results: the climatology and variability of the AEJ-AEWs
23 system from an energy point of view (3.1), climatology and variability of Saharan dust



1 aerosols across West Africa and the eastern tropical Atlantic Ocean (3.2), and the impacts
2 of dust on the AEJ-AEWs system (3.3). Conclusions are presented in Section 4.

3

4 **2 Data and methodology**

5 This study focuses on the relationships of Saharan dust aerosols and AEWs in
6 boreal summer, because during this season, the amplitude of the AEW peaks (e.g., Roundy
7 and Frank, 2004). We have applied the greater than 20-year time series of NASA's satellite
8 observations and reanalysis for the boreal summer seasons from June to August (JJA)
9 2000-2021 to calculate the variability of energy components of the system comprising the
10 AEJ, the AEWs, and aerosol radiative forcing.

11 **2.1 MODIS and MERRA-2 data**

12 To study the climatology of West Africa and the eastern tropical Atlantic Ocean,
13 the successor to the original Modern Era Retrospective-analysis reanalysis (MERRA;
14 Rienecker et al., 2008; 2011), the 3-hourly MERRA-2 (Randles et al., 1980, 2017; Buchard
15 et al., 1980; Gelaro et al., 2017) were used to provide more reliable assessments of climatic
16 and meteorological variables from 1980 to the present. The MERRA-2 reanalysis has a 3-
17 hourly temporal resolution and a spatial resolution of 0.5° latitude by 0.625° longitude with
18 72 vertical levels, extending from the surface up to 0.01-hPa.

19 We applied the MERRA-2 atmospheric radiative forcing that is broad band
20 shortwave forcing across the visible spectrum to study aerosol radiative forcing as
21 described in Section 2.2, as well as the meteorological variables, including wind
22 components, temperature, pressure and humidity from the 3-hourly MERRA-2 reanalysis



1 for the boreal summer (JJA) from 2000 to 2021, to calculate the eddy energetic terms of
2 the AEW-AEJ system as described in Section 2.3.

3 The reason for choosing the MERRA-2 analysis for this study is as follows: An
4 essential aspect of MERRA-2 is the assimilation of bias-corrected Aerosol Optical Depth
5 (AOD) and physical properties of aerosols from the various ground- and space-based
6 remote sensing platforms (e.g., Randles et al., 2017). In particular, dust is simulated in
7 MERRA-2 with a radiatively coupled version of the Goddard Chemistry, Aerosol,
8 Radiation, and Transport (GOCART; Colarco et al., 2010) aerosol model. In this manner,
9 the MERRA-2 system provides the best estimate of the atmosphere state historically from
10 the present day back to 1980.

11 To evaluate the MERRA-2 reanalysis with satellite observations, we used the
12 entire record of the daily AOD (level 3) from two independent algorithms and well-
13 calibrated sensors: (I) the 550-nm Moderate Resolution Imaging Spectro-radiometer dark-
14 target retrieval (MODIS, MOD08_D3; Remer et al., 2021 with a 1° spatial resolution on
15 Terra since 2000 for the dust domains over the Atlantic Ocean, and (II) the 470-nm Deep
16 Blue (Sayer et al., 2019; Hsu et al., 2019) retrievals of MODIS AOD available with a 1°
17 spatial resolutions for the dust source regions over the land in boreal summer (JJA, 2000-
18 2021). The summary of the information about MODIS and MERRA-2 data product name,
19 variables, special and temporal resolutions are provided in Table 1.

20

21 **2.2 Aerosol radiative forcing in the atmosphere**



1 We applied the components of aerosol radiative forcing at the surface and top of
2 the atmosphere (TOA) from the 3-hourly MERRA-2 reanalysis datasets to calculate the
3 radiative forcing of dust in the atmosphere (i.e., TOA minus surface) as follows:

$$4 \quad F_{aerosol} = (SWF_{TOA_{tot}} - SWF_{TOA_{clean}}) - (SWF_{sfc_{tot}} - SWF_{sfc_{clean}}) \quad \text{Eq. (1)}$$

5 where $SWF_{TOA_{tot}}$ refers to the net downward shortwave radiation flux at the TOA,
6 $SWF_{TOA_{clean}}$ is the net downward shortwave flux at TOA under clean-sky condition,
7 $SWF_{sfc_{tot}}$ is the net downward shortwave flux at the surface, and $SWF_{sfc_{clean}}$ is net
8 downward shortwave flux at the surface under clean-sky condition.

9 To show the variability of dust, the time-longitude Hovmöller diagrams of daily
10 anomalies of aerosol radiative forcing are provided to represent the dust transport within
11 SAL across the tropical Atlantic Ocean. The daily values of radiative forcing are calculated
12 by time averaging the 3-hourly data. The daily anomalies of radiative forcing were
13 calculated with respect to the seasonal time-average of radiative forcing for each year.
14 These anomalies were latitudinally averaged over the latitudes of dust domains, 12-22° N.

15 To investigate the relationship between dust and the AEJ-AEWs system over the
16 Atlantic Ocean, we focused on the dust variability over the ocean; therefore, we consider
17 the location of the SAL over the tropical Atlantic Ocean, the so-called OSAL domain ,
18 where dust is significant from -28° to -16° E Longitude and from 12° to 22° N latitude in
19 the climatology of boreal summer seasons.

20 **2.3 Energetics of the AEJ-AEWs system**



1 . We applied the MEERA-2 meteorological variables as described in Section 2.1,
2 to calculate the eddy energetic terms associated with the distribution of kinetic energy
3 across the AEJ-AEWs system for the boreal summer from 2000 to 2021.

4 From an energy point of view, the kinematics of the atmosphere is a combination
5 of mean kinetic energy (MKE) of the background mean flow and eddy kinetic energy
6 (EKE) representing transient eddies (Lorenz, 1954). The MKE associated with the AEJ is
7 calculated as below, where u and v are horizontal components of wind and $\bar{}$ represents
8 the time-averaged over the long-term daily time series of the wind components:

$$9 \quad MKE = \frac{1}{2}(\overline{u^2} + \overline{v^2}) \quad \text{Eq. (2)}$$

10 The following methodology was applied to detect the 2-6 day and 6-11 day
11 variations associated with the AEWs (e.g., Wu et al., 2013). While many studies have
12 focused exclusively on 2-6 day period AEWs, several studies have found evidence that
13 AEWs exist on two distinct time scales of 2-6 and 6-11 day periods, as the structure of the
14 AEWs differs substantially between these two different time windows (Mekonnen et al.
15 2006; Wu et al., 2013). The time-filtering method described below was applied to
16 decompose EKE of the AEWs at different time-scale: 2-6 day and 6-11 day filtered
17 variations.

18 We provide the daily times series of wind components by time averaging over the
19 3-hourly MERRA-2 datasets. We further used the Lanczos bandpass filtering techniques
20 described in Duchon's (1979) study to filter the 2-6 and 6-11 day disturbances from the
21 daily time series of the zonal and meridional components of wind (u, v). The daily
22 anomalies (u', v') of wind components (u, v) were calculated for each boreal summer season
23 with respect to the average of that season ($u' = u - \bar{u}$ and $v' = v - \bar{v}$; primes indicate



1 daily anomalies, and bars show seasonal averages). Finally, EKE was calculated as the
2 average of the variances of u and v shown as follows:

$$3 \quad \quad \quad EKE = 1/2 (\overline{u'^2} + \overline{v'^2}) \quad \quad \quad \text{Eq. (3)}$$

4 The bars indicate the average over the entire JJA, 2000-2021, and the primed quantities
5 denote the deviation of wind components from the time-mean (daily anomalies) described
6 above.

7 Baroclinic conversion (BCC) is one of the most important components in the eddy
8 energy budget to distribute transient energy from the upstream baroclinic source across the
9 storm tracks downstream of the jetstream (e.g., Orlanski and Katzfey, 1991; and Chang et
10 al., 2002). The initiation of and the growth of the waves are significantly related to BCC,
11 where the transient eddies extract energy from the mean-flow through BCC (e.g., Plumb,
12 1986). Following the approach described in Chang et al. (2002) study, we calculated the
13 BCC term as below:

$$14 \quad \quad \quad BCC = -\overline{\omega' \alpha'} \quad \quad \quad \text{Eq. (4)}$$

15 where ω is the rate of pressure ($\omega = \frac{dp}{dt}$) and α is a scale to estimate the changes in the
16 vertical profile of the gradient of geopotential height ($\alpha = -\frac{\partial \phi}{\partial p}$). We investigate BCC to
17 identify the locations favorable for developing EKE in the AEJ-AEWs.

18

19 **2.4 Composite analysis**

20 The composite analyses for 2-6-day and 6-11-day variations of the eddy energetics
21 of the AEWs were conducted for the boreal summer seasons of 22 years, 2000-2021.
22 Composite EKE was calculated by subtracting the EKE values associated with the lower-



1 quartile radiative forcing of dust from those EKE values associated with upper-quartile
2 aerosol radiative forcing. We find the upper- and lower-quartile aerosol radiative forcing
3 offshore, where the dust load is significant over the OSAL domain (rectangle in Figure 2a).
4 To determine the upper- and lower-quartile of aerosol forcing, the aerosol forcing over the
5 OSAL box is averaged at each time to create a time series of OSAL aerosol forcing. The
6 daily time series of aerosol radiative forcing of the grid points were spatially averaged over
7 the OSAL domain, which provided one single value of aerosol forcing for each individual
8 day in the long-term time series over the dust domain. For averaging over the OSAL
9 domain, area-weighted average is applied since the area of grid cells are not the same.
10 These time series of aerosol radiative forcing were used to select the days of the upper
11 quartile and the lower quartile aerosol radiative forcing for the summer season of each year.
12 Hence, we selected 23 days of the highest aerosol concentration (upper-quartile) and 23
13 days of the lowest aerosol concentration (lower-quartile) over each domain during boreal
14 summer of each year. From a climatology point of view, we used the upper quartile and
15 lower quartile of dust over 22 years of data, such that there are 506 data points to represent
16 the days with high values of dust concentration and 506 days with low values of dust over
17 each domain of study.

18 Composite EKE is provided for each grid point by subtracting the EKE values
19 corresponding to the upper-quartile dust days from those of the lower-quartile dust days.
20 Using the method explained above, the composite of the variance of zonal wind ($\overline{u'^2}$), the
21 variance of meridional wind ($\overline{v'^2}$), and the transient momentum fluxes ($\overline{u'v'}$) were also
22 calculated for boreal summer seasons, JJA, 2000-2001 (Figure 1).



1 2.5 Time-lag analysis

2 The time-lag analyses were conducted over each domain of study based on the
3 following processes. Using the same methodology explained above (Section 2.4.), we used
4 the time series of aerosol radiative forcing spatially averaged over the dust domain to select
5 the days in the upper quartile and the lower quartile aerosol radiative forcing, such that
6 there are 506 data points to represent the days with high values of dust concentration and
7 506 days with low values of dust concentration over each domain. For every 506 days of
8 high dust concentration, we studied the time series for five days before and five days after
9 the event to investigate the evolution of each individual dust storm. For each time series,
10 we assigned each day of 506 days as follows: $T = 0$ for the dust-peak, $T = 1$ for one day
11 after the dust-peak, $T = -1$ for one day before the peak of dust, and continue this for five
12 days before and after every 506 days. We used each of these time series for 22 years and
13 average dust radiative forcing individually for $T = 0$, $T = +/- 1$, $T = +/- 2$, $T = +/- 3$, $T = +/-$
14 4 , and $T = +/- 5$ to gain insight into the climatology of dust evolution five days before and
15 five days after dust peaks over each domain. We repeated the steps explained above for the
16 506 data points of dust in the lower quartile to provide the long-term time series of low
17 aerosol radiative forcing over the dust domain. Finally, by subtracting the time series of
18 the lower quartile from the upper quartile radiative forcing, we provide the composite of
19 dust over each domain to investigate the highest variability of dust (as $T = 0$, Figure 5) and
20 its evolution five days before and after over dust domain. Using the same methodology, we
21 analyzed the wave activity that coincides with the upper quartile (and lower quartile)
22 aerosol radiative forcing to investigate a possible time-lag between the dust and the



1 development of kinetic energy over the northern and southern track of the AEWs. The
2 domains selected to investigate wave activity are shown in Table 2.

3

4 **3 Summary of the results**

5 **3.1 AEJ-AEWs system from an energy perspective**

6 Traditional studies have used the mid-tropospheric trough and ridge from unfiltered
7 wind fields to diagnose the AEWs. In this manner, the AEWs trough was identified where
8 the meridional wind at the vertical level of the AEJ is equal to zero, indicating that the wind
9 shifts from northerlies to southerlies (Diedhiou et al., 1999). The existence of two distinct
10 tracks of the AEWs: the northern and southern tracks (e.g., Diedhiou et al., 1999; Nitta and
11 Takayabu, 1985; Reed et al., 1988; Wu et al., 2013) have been identified by examining the
12 vorticity structure of the AEWs (e.g., Carlson 1969 a&b; Thorncroft and Hodges, 2001;
13 Hopsch et al., 2007) and applying the reversal of the meridional gradient of potential
14 vorticity (e.g., Norquist et al., 1977; Pytharoulis and Thorncroft, 1999; Kiladis et al., 2006).
15 However, these methods are limited because of the overlapping scale of AEWs with other
16 phenomena and the significant amount of manual intervention required to differentiate
17 between synoptic-scale AEW trough axes and localized circulation centers. As a solution
18 to this problem, here we applied the eddy energy budget to diagnose the growth and
19 evolution of the AEWs.

20 Hosseinpour and Wilcox (2014) showed that the axis of the AEJ core resides at
21 about 600-hPa during the boreal summer; thus, here we present the results for 600-hPa,
22 where the activity of the AEJ-AEWs system is maximized. Figure 1a shows the mid-level
23 AEJ in the climatology of boreal summer. The core of the jet is zonally located from 20°



1 E to 30° W between the Sahel and the Sahara and spans from Africa toward the Atlantic
2 Ocean, where the jet axis is located at ~15° N latitude. The closed contours in Figure 1b-c
3 represent the MKE of the AEJ. The MKE peaks at ~12-18° N, collocated with the core of
4 the AEJ (Figure 1a). The long-term mean of the mid-level EKE for the 2-6-day (warm
5 shades in Figure 1b) and 6-11-day (warm shades in Figure 1c) bandpass filtered EKE
6 represents the kinetic energy of two distinct categories of the AEWs: The 2-6-day bandpass
7 EKE peaks offshore, downstream and along the northern side of the jet core, while the 6-
8 11-day bandpass EKE has a weaker signal over the northern side of the jet compared to 2-
9 6-day EKE. The significant signal of the 2-6-day AEWs over the tropical Atlantic implies
10 the significant contribution of 2-6-day transient eddies in transient disturbances over the
11 Ocean.

12 In addition, both 2-6-day and 6-11-day bandpass EKE can develop at the higher
13 latitudes above ~32° N toward the subtropics, which can be related to the impacts of the
14 westerly Rossby waves of the subtropical storm track over North Africa. These are
15 consistent with the previous studies, showing that after leaving the West coast of Africa,
16 the majority of AEWs either (1) penetrate the subtropical Atlantic Ocean via an interaction
17 with an extratropical trough, or (2) develop further downstream and are involved in tropical
18 cyclogenesis (Berry et al., 2007; Chen et al., 2008).

19 **3.1.1 Behaviors of transient eddies of the AEWs**

20 In this Section, we further investigate the characteristics of the AEWs. Figures 1d
21 and 1e show the climatology of transient eddies. The variance of zonal wind ($\overline{u'^2}$)
22 represents the zonal transient eddies (Figure 1d), which peak at ~6-12° N and are elongated



1 downstream along the southern edge of the AEJ from approximately 15° W to 45° W.
2 Comparing this with Figure 1b shows that the increase of 2-6-day bandpass EKE
3 downstream of the jet core corresponds to the 2-6-day zonal transient eddies, whereas the
4 core of the 2-6-day EKE over the northern track AEWs at ~18-24° N is related to the
5 meridional wind variance ($\overline{v'^2}$), which represents the 2-6-day meridional transient eddies
6 (Figure 1e). These patterns suggest that transient eddies of the 2-6-day time-scale AEWs
7 are elongated both zonally and meridionally.

8 Figure 1f gives further information about the structure and propagation of the 2-6-
9 day eddies. The enhanced transient momentum flux ($\overline{u'v'}$) of 2-6-day bandpass eddies over
10 the northern and southern tracks of the AEWs indicates the orientation and the group
11 velocity of the transient eddies relative to easterly mean-flow. The positive values of the
12 transient momentum flux are dominant over the southern sides of the jet core, suggesting
13 that the southern track transient eddies propagate with a NE-SW orientation, whereas the
14 negative values of the transient momentum flux over the northern track suggest the NW-
15 SE orientation of transient eddies relative to the mean-flow. The relatively tilted
16 orientations of the eddies over the northern and southern track, fanning out or diverging
17 downstream of the jet core, are signatures of the so-called downstream development, where
18 transient eddy activity associated with 2-6-day AEWs is enhanced. The magnitude of the
19 transient momentum flux shows the 2-6-day eddies over the northern and southern tracks
20 of the AEWs propagate faster relative to the easterly mean-flow, whereas the values of
21 transient momentum flux are negligible along the AEJ axis where the mean-flow is strong.
22 To further investigate the behavior of the 2-6-day eddies, we discuss the baroclinic and
23 barotropic instability of the waves in the following Section.



1 **3.1.2 Baroclinic instability of the AEJ-AEWs system**

2 Baroclinic instability is the dynamic cause for synoptic-scale storms as a result of
3 vertical shear of the zonal wind, corresponding to meridional temperature gradients based
4 on the thermal wind balance (e.g., Charney, 1947; Eady, 1949). Meridional temperature
5 gradient is also proportional to the available potential energy in baroclinic instability
6 mechanism (Hoskins et al., 1983; Grotjahn, 2003). Baroclinic zones are defined as the
7 favored areas for strengthening and weakening of systems, where eddies extract available
8 potential energy from the mean-flow and convert the eddy available potential energy to
9 EKE through baroclinic conversion (BCC) of energy (Chang et al., 2002; Orlanski and
10 Katzfey, 1991). The changes in meridional temperature gradient also contribute to the
11 changes in EKE of the waves (e.g., Coumou et al., J., 2015; Gertler and O’Gorman, 2019).

12 Previous studies showed that $\overline{u'v'}$ is an indicator of baroclinic instability at the exit
13 region of the jet (e.g., Hoskins et al., 1983). Figure 1f represents the presence of baroclinic
14 instability ($\overline{u'v'}$) at the northern and southern tracks of the waves downstream of the jet
15 core, showing the development of the 2-6-day transient eddy activity downstream of the
16 AEJ corresponds to the presence of baroclinic instability in the region where eddies can
17 extract energy from the easterly mean-flow through baroclinic conversion (as described in
18 the following Section). These suggest that the northern and southern tracks of the AEWs
19 are favorable areas for the potential growth of baroclinic transient eddies as the variations
20 in baroclinic instability tend to extract energy from the jet and convert it to eddy energy
21 downstream of the AEJ, where the jet weakens.

22 We further investigated the conversion of energy through BCC by studying the
23 fraction of the total variance of BCC (Figure 1g) attributable to variations on less than 11-



1 day time scales, which includes both the 2-6-day AEWs and 6-11-day AEWs. Figure 1g
2 shows that these variations account for a significant fraction of BCC variations over land,
3 where the AEJ core resides (Figure 1a), and this high fraction of BCC variance extends
4 offshore over the northern and southern sides of the AEJ. This is consistent with the
5 discussion above, suggesting the eddy activity occurs at the north and south sides of the
6 AEJ (Figure 1f), where the transient zonal and meridional eddies (Figures 1d-e) extract
7 energy from the MKE (contours in Figure 1b-c) and convert it to EKE (Figure 1b-c)
8 through BCC.

9 In the next Section, we investigated the relationships between the African aerosols
10 and the AEWs. Studying the time series of EKE and dust anomalies shows a similarity
11 between the variability of dust radiative forcing and the changes of the 2-6-day EKE over
12 the northern and southern tracks of the AEWs (Figures S1 and S2), suggesting a possible
13 impact of dust diabatic heating on the enhancement of the kinetic energy of the AEWs.
14 Such a relationship between dust and AEWs is also seen over each individual JJA (Figure
15 S3). We explore Saharan dust variability (Section 3.2) and then investigate the possible
16 impacts of aerosol radiative forcing of dust concentration on the energy of AEWs (Section
17 3.3).

18

19 **3.2 Saharan dust plumes- climatology and variability**

20 The significant dust transport from the Saharan desert across the Atlantic Ocean is
21 seen in the long-term mean of Saharan dust optical thickness and radiative forcing
22 vertically integrated over the troposphere during boreal summer (Figures 2a-c). The
23 inherent limitation of MODIS satellite observations is the lack of AOD data over the



1 highly-reflective desert regions (Figure 2a) and the Deep Blue AOD over the Ocean (Figure
2 2b). Because of that, based on Eq. (1) we calculated aerosol shortwave radiative forcing
3 from the MERRA-2 reanalysis as a complementary component (Figure 2c) to the satellite
4 observations. This was further examined by the scatter plots of MODIS AOD over the
5 Ocean (Figure 2d) and Deep Blue over the land (Figure 2e) with respect to MERRA-2
6 radiative forcing, where daily data points were averaged over the oceanic and land dust
7 domains (rectangle in Figures 2a and 2b, respectively). This shows that MERRA-2
8 reanalysis is highly correlated with MODIS observations with R-values of 0.83 and 0.62,
9 respectively, and statistically significant with P-values less than 0.05. From a climatology
10 point of view, the maximum value of dust heating the atmosphere is approximately 35 Wm^{-2}
11 2 , localized over the western and central Saharan Desert in JJA, 2000-2021 (Figure 2c).
12 The maximum value is roughly similar for each individual JJA (not shown). In addition,
13 the radiative forcing efficiency for atmospheric heating by Saharan dust inferred from these
14 scatter plots (Figures 2d-e) is roughly 20 Wm^{-2} per unit AOD over the ocean and 35 Wm^{-2}
15 per unit AOD over land.

16 We investigated dust variability by studying the changes in daily radiative forcing
17 during dust transport across the tropical Atlantic Ocean. The longitude-time Hovmöller
18 diagrams of daily aerosol radiative forcing anomalies are provided for each summer from
19 2000 to 2021 (Figure 3). The aerosol radiative forcing is meridionally averaged over the
20 SAL, 12-22°N, where the dust concentration is high. The positive and negative anomalies
21 show the increase and decrease of aerosol radiative forcing within the SAL as dust
22 propagates in transient dust plumes across the tropical Atlantic Ocean. Figure 3 shows that,
23 on average, dust transport may reach the Caribbean Sea in less than 11 days. To investigate



1 the climatology of this, the fraction of total variance of dust radiative forcing was calculated
2 for less than 11-day and more than 11-day of dust variations during boreal summer seasons,
3 2000-2021 (Figures 2f-g). The variations of aerosol radiative forcing for less than 11-day
4 timescale variations are significant over West Africa and the eastern tropical Atlantic
5 Ocean and account for up to 70-80% of the total variance of aerosol radiative forcing over
6 these regions. In contrast, the variations of dust radiative forcing longer than 11-day are a
7 more significant fraction of the variance upstream, mainly over the dust sources in the
8 Saharan Desert.

9 We conducted similar Hovmöller analyses as above, but for MODIS observations
10 as a check on the dust forcing variability in the MERRA-2 reanalysis and found that the
11 results from MERRA-2 reanalysis were consistent with the MODIS AOD (Figure S3).
12 Analyzing the dust storm events from 2000 to 2021 suggests a possible relationship
13 between the dust transport and the variations of the AEJ-AEWs system. Our hypothesis is
14 that the variations of dust across the ocean during Saharan dust storms contribute to the
15 growth of the waves over the ocean through diabatic heating from dust radiative forcing.
16 To investigate this, we focus on the dust over the oceanic domain (i.e., OSAL; rectangle in
17 Figure 2a). The steps to study this are described in the following sections.

18 **3.3 Impacts of dust radiative forcing on the energy of the AEWs**

19 Previous studies have discussed the dynamics of the AEWs as summarized in the
20 introductory Section; however, the relationships between dust radiative forcing and the
21 kinetic energy of the AEWs are still unexplored. In this Section, we investigate the



1 relationships between dust radiative forcing of the atmosphere (TOA minus surface) and
2 the kinetic energy of the AEWs during the boreal summer from 2000 to 2021.

3 **3.3.1 Composite analysis of eddy energetics with respect to dust variability**

4 The composite analyses were conducted for the boreal summer seasons of 22 years.
5 The composite of the 2-6-day and 6-11-day filtered EKE (Figures 4a and 4b, respectively)
6 are based on the EKE values for the times that correspond to the upper-quartile dust
7 radiative forcing in the OSAL region (rectangle in Figure 2a) minus the EKE values of the
8 times correspond to the lower-quartile dust radiative forcing. The steps to calculate
9 composite diagrams are explained in Section 2.

10 The positive anomalies in Figure 4a show the increase of the 2-6-day EKE at the
11 southern track (~ 6-12°N) of the AEWs and further downstream over the northern track (~
12 18-24°N) coincide with the enhanced radiative forcing of dust over the offshore region.
13 The dipole pattern of the positive and negative anomalies may also imply a possible
14 southward shift of the 2-6-day EKE at the southern edge of the AEJ during high dust
15 concentrations. A similar dipole pattern can also be seen in Figure 4c.

16 Figure 4c shows the increase of the zonally elongated 2-6-day eddies at the southern
17 edge of the jet, which suggests that the strengthening of the 2-6-day zonal transient eddies
18 may lead to the amplification of EKE (Figure 4a) over the southern track of the waves
19 during dust events when aerosol radiative forcing is significant offshore. Meanwhile, the
20 increase of the meridional elongated transient eddies (Figure 4d) coincides with the high
21 concentrations of dust. Comparing this with Figure 4a suggests that during high dust
22 concentration in OSAL, the amplification of the 2-6-day EKE further downstream in the



1 northern track of the AEWs corresponds to the enhanced meridional elongated transient
2 eddies. While the positive anomalies of 2-6-day $\overline{u'v'}$ (Figure 4e) is a weaker signal at the
3 northern and southern tracks of the waves, it is still statistically significant, which shows
4 that the enhancement of the baroclinic instability over the northern and southern tracks of
5 the AEWs occurs during high aerosol radiative forcing in OSAL.

6 The negative composite along the AEJ axis at about 12-18°N (Figure 4) can be
7 related to the fact that the 2-6-day and 6-11-day EKE are not significant along the AEJ
8 axis, where the MKE and the horizontal shear of mean-flow are strong (Figure 1a-b-c). As
9 described in Section 3.1., the growth of transient eddies is more likely over the south and
10 north side of the jet, where the jet weakens and thus offers a greater chance for the
11 development of baroclinic AEWs (Figure 1f-g). While the negative anomaly may seem
12 like a reduction of eddy activity along the AEJ axis simultaneously at the time of dust
13 enhancement, in the next Section (3.3.2), we have evidence that the amplification of 2-6-
14 day EKE along the AEJ axis starts on average two days after the peak of dust offshore
15 (Figures 5 d-e).

16 We conducted the same composite analysis using MODIS AOD, which shows that
17 the results are consistent whether the MERRA-2 radiative forcing metric or the MODIS
18 AOD data are applied (Figure S4). Overall, these composite analyses suggest a mechanistic
19 relationship between the kinetic energy of the AEJ-AEWs system over the ocean and
20 aerosol radiative forcing during dust outbreaks in summer. The enhanced dust offshore
21 coincides with the strengthening of the baroclinic instability and amplification of the 2-6-
22 day AEWs downstream, where the jet weakens and gives a chance to strengthen the
23 propagation of the zonally and meridionally elongated transient eddies over the southern



1 and northern tracks of the waves, respectively. In the following Section, we study a possible
2 time lag between the occurrence of dust storms and the changes in the activity of the waves
3 over various domains.

4

5 **3.3.2 Time-lag between dust outbreaks and development of the AEWs**

6 In this Section, we investigate a possible lag between the changes of the EKE with
7 respect to the variability of dust radiative forcing over the OSAL. We divide the northern
8 track waves (18° to 24° N) and southern track (6° to 12° N) of the AEWs into two separate
9 regions: Eastern Atlantic (-15° to -30° E) and Central Atlantic (-30° to -45° E). We also
10 study the possible lag between dust in OSAL and the eddy activity downstream of the jet
11 core (12° to 18° N) over the eastern and central Atlantic domains (Table 2). The time lag is
12 investigated between composite EKE over each wave domain with respect to composite
13 dust radiative forcing in OSAL. The methodology for calculating time lag is described in
14 Section 2.

15 The variability of dust radiative forcing (i.e., composite for daily upper quartile
16 aerosol radiative forcing minus daily lower quartile aerosol radiative forcing) in Figure 5a
17 represents the daily variations of radiative forcing five days before and after the peak of
18 dust in the OSAL region for the 22 years of boreal summer seasons. This shows the
19 variability of dust radiative forcing associated with the dust outbreaks over the OSAL
20 region is significant for about six days, as it starts three days before ($T = -3$) and ends three
21 days after ($T = +3$) the peak of dust ($T = 0$), which is consistent with the timescale of the
22 2-6-day AEWs. Similar analyses are conducted using the upper quartile radiative forcing



1 only to investigate such relationships for the days with high dust concentration (Figure S5).
2 The results are consistent with the patterns shown in Figure 5.

3 Figures 5b represents the time evolution and changes in 2-6-day EKE of the
4 northern track AEWs further downstream over the eastern Atlantic Ocean. The changes in
5 EKE seem negligible at $T < 0$ before starting the high variations in dust in OSAL; however,
6 the growth of EKE occurs on average at $T = 0$, coinciding with the peak of dust, and then
7 continues growing and reaches its maximum about three days ($T = +3$) after the peak of
8 dust variations. In contrast, although a slight decrease and increase of EKE are seen
9 respectively before and after dust peaks, the variations of the northern track EKE over the
10 eastern Atlantic (Figure 5c) seem weaker compared to those further downstream.
11 Comparing Figure 5b with the composite analysis in Figure 4a suggests that the
12 enhancement of the northern track 2-6-day EKE, further downstream over the central
13 Atlantic, coincides with the peak of dust and is even more significant on average three days
14 after dust peaks in OSAL.

15 The negative variations of the EKE in Figures 5d and 5e at $T = 0$ are consistent with
16 the negative composite of the EKE along the AEJ axis in Figure 4. This means that the
17 decay of EKE along the jet axis over the Central Atlantic (Figure 5d) is initiated before
18 dust activity; however, the rapid growth of EKE starts on average two days ($T = +2$) after
19 the peak of dust and is maximized about three to four days ($T \sim +3$ to $+4$) after the peak of
20 dust in OSAL. A similar, but weaker pattern, is seen across the jet axis over the eastern
21 Atlantic (Figure 5e).

22 Figures 5f and 5g show that the changes in EKE are maintained positive before and
23 after dust activity. Comparing Figure 5f with Figure 5a suggests that the activity of both



1 dust plumes in OSAL and the southern EKE anomalies over the central Atlantic is initiated
2 about three days ($T = -3$) before dust peaks, and then amplification of EKE continues and
3 reaches its maximum on average two days ($T = +2$) after dust peaks.

4 Over the eastern tropical Atlantic (Figure 5g), the EKE variations seem negligible
5 during dust storms. The weaker signal of the southern track EKE variations over the eastern
6 Atlantic can be explained by the dynamic and energy of the AEJ-AEWs system (Figure 1),
7 as this is the region where the southern edge of the jet is dominant, and the MKE and
8 conversion of energy to EKE through BCC are significant. This suggests that while the
9 positive anomalies of EKE over this region coincide with the enhancement of dust in
10 OSAL, the influence of dust radiative forcing on changes in EKE could be weak
11 quantitatively compared to the amount of energy exchange between the components of the
12 AEJ-AEWs system at the southern edge of the jet core.

13 Comparing Figures 5b, 5d, and 5f reveals evidence of the mechanistic relationship
14 between variability of dust radiative forcing offshore and the changes in the 2-6-day EKE
15 further downstream over the Central tropical Atlantic, where the easterly flow weakens at
16 the exit region of the jet over the central Atlantic. On average, the peak of dust load in
17 OSAL occurs a few days before the amplification of the EKE downstream of the AEJ; a
18 similar pattern is also seen with a weaker signal over the eastern tropical Atlantic. The lag
19 analyses, summarized in Table 3, suggest that the peak of dust aerosols loading offshore
20 over the OSAL region precedes the amplification of EKE further downstream of the AEJ
21 over the central Atlantic Ocean. This evidence is consistent with our hypothesis on the
22 influence of dust radiative forcing, fueling the EKE of the 2-6-day AEWs downstream of
23 the AEJ over the tropical Atlantic Ocean, where tropical cyclogenesis and hurricane



1 activity occur. We further investigated our analyses by selecting various dust domains (e.g.,
2 12° to 22°N and -38° to -28°E, shown in Figure S6) and showed that our findings are
3 consistent regardless of the location of dust domain in SAL across the tropical Atlantic
4 Ocean.

5

6 **4 Conclusions**

7 While previous studies showed the relationship between dust transport and AEJ and
8 AEWs across the Atlantic Ocean (Perry et al., 1997; Liu et al., 2008; Francis et al., 2020;
9 Francis et al., 2021) the feedback of dust to AEJ-AEW is not well understood. A few recent
10 studies showed that dust affects the atmospheric dynamics of the Atlantic Ocean by
11 enhancing AEJ and AEW strength (e.g., Bercos-Hickey et al., 2017; Grogan et al., 2016).
12 However, the mechanisms of such effects are still open questions.

13 This study shows mechanistic relationships between the radiative forcing of dust
14 aerosols in SAL and the kinetic energy of the AEWs across the tropical Atlantic Ocean
15 using 22 years of daily satellite observations, as well as reanalysis data based on satellite
16 assimilation. Dust plumes across the Atlantic are not merely transported by AEJ-AEWs
17 system but also contribute to increasing the kinetic energy of the baroclinic AEWs through
18 diabatic heating. The enhanced dust contributes to an increase in meridional temperature
19 gradients, which leads to an increase in baroclinicity and amplification of the EKE of the
20 AEWs.

21 The radiative forcing efficiency of dust in the atmosphere is a heating of roughly
22 20 Wm⁻² per unit AOD over the ocean and 35 Wm⁻² per unit AOD over land. This agrees
23 with in-situ measurements (Soupiona et al., 2020) and regional climate modeling (Saidou



1 Chaibou et al., 2020) of Saharan dust radiative forcing. This radiative forcing of dust
2 aerosols in the SAL contributes to the diabatic heating of the atmosphere in the regions
3 where the increase in temperature gradients leads to the growth of baroclinic waves through
4 the conversion of energy to EKE in the AEJ-AEWs system. Outbreaks of high dust
5 concentrations in the SAL coincide with the growth of the meridionally elongated 2-6-day
6 transient eddies over the northern track of AEWs (~18-24°N) and zonally elongated eddies
7 over the southern track of AEWs (~6-12°N). This leads to amplifying the EKE of the
8 AEWs, particularly at the exit region of the AEJ, where the MKE and the horizontal shear
9 of mean-flow are weakened. This offers the chance for downstream development of the
10 AEWs, associated with enhanced dust. The dust-induced enhancement of AEW through a
11 buoyancy source was shown by Grogan et al. (2016), albeit with a different methodology
12 (i.e., analytical and regional modeling analyses). In addition, our results agree with a case
13 study of the Saharan dust event by a regional climate model (Bercos-Hickey et al., 2017)
14 that showed that Saharan dust causes AEW to shift northward and expand westward.

15 The growth of the baroclinic transient eddies, and the corresponding EKE of the 2-
16 6-day AEWs, is amplified at the exit region of the AEJ, on average, two to four days after
17 the enhancement of dust upstream in the OSAL region. Our findings show that dust activity
18 precedes the amplification of EKE, suggesting that the diabatic heating from dust radiative
19 forcing can fuel the development of the AEWs. This mechanistic impact of dust radiative
20 forcing onto AEW development is consistent across the tropical Atlantic Ocean. This study
21 further supports a cause-and-effect hypothesis between dust radiative forcing and transient
22 wave dynamics that may be tested in sensitivity studies with dynamical climate models to
23 explore further the cause and effect of such relationships.



1

2 **Acknowledgments**

3 This work is supported by the NASA Interdisciplinary Science Program through grants
4 #NNX11AF21G and #NNX14AH95G. Special thanks to Drs. Hans Moosmuller and
5 Naresh Kumar for their comments that contributed to the improvement of this manuscript.
6 We also appreciate the anonymous reviewers for their constructive comments.

7

8 **Data availability**

9 MERRA-2 aerosol, radiation, and meteorological datasets can be obtained from
10 <https://disc.gsfc.nasa.gov/datasets>. MODIS AOD retrievals are accessible through
11 <https://modis.gsfc.nasa.gov/data/dataproduct/mod04.php>. Numerical codes developed to
12 conduct data extraction, analysis, and visualization will be provided upon request.

13

14

15 **Author contributions**

16 FH and EW originated this study. FH formulated, developed and implemented the codes,
17 and analyzed the results with inputs from EW. FH drafted the paper, and EW provided
18 edits and revisions.

19

20 **Competing interests**

21 The authors have no competing interests.

22



1 **References**

- 2 Avila, L. A., & Clark, G. B., 1989. Atlantic Tropical Systems of 1988, *Monthly Weather*
3 *Review*, 117(10), 2260-2265, [https://doi.org/10.1175/1520-](https://doi.org/10.1175/1520-0493(1989)117%3C2260:ATSO%3E2.0.CO;2)
4 [0493\(1989\)117%3C2260:ATSO%3E2.0.CO;2](https://doi.org/10.1175/1520-0493(1989)117%3C2260:ATSO%3E2.0.CO;2)
- 5 Avila, L. A., & Pasch, R. J. 1992. Atlantic Tropical Systems of 1991, *Monthly Weather*
6 *Review*, 120(11), 2688-2696, [https://doi.org/10.1175/1520-](https://doi.org/10.1175/1520-0493(1992)120<2688:ATSO>2.0.CO;2)
7 [0493\(1992\)120<2688:ATSO>2.0.CO;2](https://doi.org/10.1175/1520-0493(1992)120<2688:ATSO>2.0.CO;2)
- 8 Barbosa, P.M., Stroppiana, D., Grégoire, J.M. and Cardoso Pereira, J.M., 1999. An
9 assessment of vegetation fire in Africa (1981–1991): Burned areas, burned biomass, and
10 atmospheric emissions. *Global Biogeochemical Cycles*, 13(4), pp.933-
11 950, <https://doi.org/10.1029/1999GB900042>
- 12 Bercos-Hickey, E., Nathan, T. R., & Chen, S. H. (2017). Saharan dust and the African
13 easterly jet-African easterly wave system: Structure, location and energetics, *QJ Roy.*
14 *Meteor. Soc.*, 143, 2797–2808. <https://doi.org/10.1002/qj.3128>
- 15 Bercos-Hickey, E., T. R. Nathan, and S.-H. Chen, 2020. On the Relationship between the
16 African Easterly Jet, Saharan Mineral Dust Aerosols, and West African Precipitation. *J.*
17 *Clim.*, 2020, 33, 3533–3546, <https://doi.org/10.1175/jcli-d-18-0661.1>
- 18 Bercos-Hickey, E., & Patricola, C. M. (2021). Anthropogenic influences on the African
19 easterly jet–African easterly wave system. *Climate Dynamics*, 57(9-10), 2779-2792.
20 <https://doi.org/10.1007/s00382-021-05838-1>
- 21 Berry, G., C. D. Thorncroft, and T. Hewson, 2007. African easterly waves during 2004—
22 Analysis using objective techniques. *Mon. Wea. Rev.*, **135**, 1251–1267,
23 <https://doi.org/10.1175/MWR3343.1>
- 24 Berry G. J. and C.D. Thorncroft, 2012. African easterly wave dynamics in a mesoscale
25 numerical model: The upscale role of convection *J. Atmos. Sci.*, 69, 1267–1283,
26 <https://doi.org/10.1175/JAS-D-11-099.1>



- 1 Buchard, V., et al., 2017. The MERRA-2 Aerosol Reanalysis, 1980 Onward. Part II:
2 Evaluation and Case Studies, *Journal of Climate*, 30(17), 6851-6872,
3 <https://doi.org/10.1175/JCLI-D-16-0613.1>
- 4 Cahoon, D.R., Stocks, B.J., Levine, J.S., Cofer, W.R. and O'Neill, K.P., 1992. Seasonal
5 distribution of African savanna fires. *Nature*, 359(6398), pp.812-815,
6 <https://doi.org/10.1038/359812a0>
- 7 Carlson, T. N., 1969. Synoptic histories of three African disturbances that developed into
8 Atlantic hurricanes. *Mon. Wea. Rev.*, 97, 256–276.
- 9 Carlson, T.N. and Prospero, J.M., 1972. The Large-Scale Movement of Saharan Air
10 Outbreaks over the Northern Equatorial Atlantic. *Journal of Applied Meteorology*, 11,
11 283-297.
12 [https://doi.org/10.1175/1520-0450\(1972\)011<0283:TLSMOS>2.0.CO;2](https://doi.org/10.1175/1520-0450(1972)011<0283:TLSMOS>2.0.CO;2)
- 13 Chang, C. B., 1993. Impact of desert environment on the genesis of African wave
14 disturbances. *J. Atmos. Sci.*, **50**, 2137–2145.
- 15 Chang E. K. M., S. Lee and K. L. Swanson, 2002. Storm track dynamics. *J. Climate*, 15,
16 2163–2183, [https://doi.org/10.1175/1520-0442\(2002\)015<02163:STD>2.0.CO;2](https://doi.org/10.1175/1520-0442(2002)015<02163:STD>2.0.CO;2)
- 17 Charney, J. G., 1947. The Dynamics of Long Waves in a Baroclinic Westerly Current,
18 *Journal of Atmospheric Sciences*, 4(5), 136-162.
19 [https://journals.ametsoc.org/view/journals/atsc/4/5/1520-](https://journals.ametsoc.org/view/journals/atsc/4/5/1520-0469_1947_004_0136_tdolwi_2_0_co_2.xml)
20 [0469_1947_004_0136_tdolwi_2_0_co_2.xml](https://journals.ametsoc.org/view/journals/atsc/4/5/1520-0469_1947_004_0136_tdolwi_2_0_co_2.xml)
- 21 Charney, J. G., and M. E. Stern, 1962. On the stability of internal baroclinic jets in a
22 rotating atmosphere. *J. Atmos. Sci.*, **19**, 159–172.
- 23 Chen, T., Wang, S., & Clark, A. J. 2008. North Atlantic Hurricanes Contributed by
24 African Easterly Waves North and South of the African Easterly Jet, *Journal of*
25 *Climate*, 21(24), 6767-6776, <https://doi.org/10.1175/2008JCLI2523.1>



- 1 Chen, S. H., McDowell, B., Huang, C. C., & Nathan, T. R., 2021. Formation of a low-
2 level barrier jet and its modulation by dust radiative forcing over the Hexi Corridor in
3 Central China on March 17, 2010. *Quarterly Journal of the Royal Meteorological*
4 *Society*, 147(736), 1873-1891
- 5 Cochrane, S. P., Schmidt, K. S., Chen, H., Pilewskie, P., Kittelman, S., Redemann, J.,
6 LeBlanc, S., Pistone, K., Segal Rozenhaimer, M., Kacenelenbogen, M., Shinozuka, Y.,
7 Flynn, C., Ferrare, R., Burton, S., Hostetler, C., Mallet, M., and Zuidema, P.: Biomass
8 burning aerosol heating rates from the ORACLES (ObseRvations of Aerosols above
9 CLouds and their intEractionS) 2016 and 2017 experiments, *Atmos. Meas. Tech.*, 15, 61–
10 77, <https://doi.org/10.5194/amt-15-61-2022>, 2022.
- 11 Colarco, P. R., Toon, O. B., and Holben, B. N., 2003. Saharan dust transport to the
12 Caribbean during PRIDE: 1. Influence of dust sources and removal mechanisms on the
13 timing and magnitude of downwind aerosol optical depth events from simulations of in
14 situ and remote sensing observations, *J. Geophys. Res.*, 108, 8589,
15 doi:10.1029/2002JD002658.
- 16 Colarco, P., A. da Silva, M. Chin, and T. Diehl, 2010. Online simulations of global
17 aerosol distributions in the NASA GEOS-4 model and comparisons to satellite and
18 ground-based aerosol optical depth. *J. Geophys. Res.*, 115, D14207,
19 <https://doi.org/10.1029/2009JD012820>.
- 20 Cornforth R. J., B. J. Hoskins, and C. D. Thorncroft, 2009. The impact of moist processes
21 on the African easterly jet–African easterly wave system *Q. J. R. Meteorol. Soc.* 135,
22 894–913, <https://doi.org/10.1002/qj.414>.
- 23 Coumou, D., Lehmann, J., & Beckmann, J., 2015. The weakening summer circulation in
24 the Northern Hemisphere mid-latitudes. *Science*, 348(6232), 324-327.
- 25 Dee, D.P., et al., 2011. The ERA-Interim reanalysis: configuration and performance of
26 the data assimilation system. *Q.J.R. Meteorol. Soc.*, 137: 553-
27 597. <https://doi.org/10.1002/qj.828>



- 1 Diaz, M. and Aiyyer, A., 2013. The Genesis of African Easterly Waves by Upstream
- 2 Development. *Journal of the Atmospheric Sciences*, 70, 3492-3512.

- 3 Diedhiou, A., et al., 1999. Easterly wave regimes and associated convection over West
- 4 Africa and tropical Atlantic: results from the NCEP/NCAR and ECMWF
- 5 reanalyses. *Climate Dynamics* 15, 795–822, <https://doi.org/10.1007/s003820050316>

- 6 Duchon C. E., 1979. Lanczos filtering in one and two dimensions, *J. Appl.*
- 7 *Meteorol.*, 18, 1016–1022, [https://doi.org/10.1175/1520-](https://doi.org/10.1175/1520-0450(1979)018<1016:LFIOAT>2.0.CO;2)
- 8 [0450\(1979\)018<1016:LFIOAT>2.0.CO;2](https://doi.org/10.1175/1520-0450(1979)018<1016:LFIOAT>2.0.CO;2).

- 9 Dunn G. E., 1940. Cyclogenesis in the tropical Atlantic. *Bull. Amer. Meteor. Soc.*, 21,
- 10 215–229.

- 11 Eady, E.T., 1949. Long Waves and Cyclone Waves. *Tellus*, 1: 33-52.
- 12 <https://doi.org/10.1111/j.2153-3490.1949.tb01265.x>

- 13 Francis, D., Fonseca, R., Nelli, N., Cuesta, J., Weston, M., Evan, A., & Temimi, M.
- 14 (2020). The atmospheric drivers of the major Saharan dust storm in June
- 15 2020. *Geophysical Research Letters*, 47(24), e2020GL090102.
- 16 <https://doi.org/10.1029/2020GL090102>

- 17 Francis, D., Nelli, N., Fonseca, R., Weston, M., Flamant, C., & Cherif, C. (2022). The
- 18 dust load and radiative impact associated with the June 2020 historical Saharan dust
- 19 storm. *Atmospheric Environment*, 268, 118808.
- 20 <https://doi.org/10.1016/j.atmosenv.2021.118808>

- 21 Gelaro, R., McCarty, W., Suárez, M. J., Todling, R., Molod, A., Takacs, L., et al., 2017.
- 22 The modern-era retrospective analysis for research and applications, version 2 (MERRA-
- 23 2). *J. Clim.*, 30(14), 5419-5454.

- 24 Gertler, C. G., & O’Gorman, P. A., 2019. Changing available energy for extratropical
- 25 cyclones and associated convection in Northern Hemisphere summer. *Proceedings of the*
- 26 *National Academy of Sciences*, 116(10), 4105-4110.



- 1 Global Modeling and Assimilation Office (GMAO) (2015a), MERRA-2
- 2 inst6_3d_ana_Np: 3d,6-Hourly,Instantaneous,Pressure-Level,Analysis,Analyzed
- 3 Meteorological Fields V5.12.4, Greenbelt, MD, USA, Goddard Earth Sciences Data and
- 4 Information Services Center (GES DISC), doi.org/10.5067/A7S6XP56VZWS

- 5 Global Modeling and Assimilation Office (GMAO) (2015b), MERRA-2
- 6 tag1_2d_rad_Nx: 2d,1-Hourly,Time-Averaged,Single-Level,Assimilation,Radiation
- 7 Diagnostics V5.12.4, Greenbelt, MD, USA, Goddard Earth Sciences Data and
- 8 Information Services Center (GES DISC), [10.5067/Q9QMY5PBNV1T](https://doi.org/10.5067/Q9QMY5PBNV1T)

- 9 Global Modeling and Assimilation Office (GMAO) (2015c), MERRA-2
- 10 inst3_3d_asm_Np: 3d,3-Hourly,Instantaneous,Pressure-Level,Assimilation,Assimilated
- 11 Meteorological Fields V5.12.4, Greenbelt, MD, USA, Goddard Earth Sciences Data and
- 12 Information Services Center (GES DISC), [10.5067/QBZ6MG944HW0](https://doi.org/10.5067/QBZ6MG944HW0)

- 13 Grogan, D. F., Nathan, T. R., & Chen, S. H. (2016). Effects of Saharan dust on the linear
- 14 dynamics of African easterly waves. *Journal of the Atmospheric Sciences*, 73(2), 891-
- 15 911. <https://doi.org/10.1175/JAS-D-15-0143.1>

- 16 Grogan, D. F., Nathan, T. R., & Chen, S. H. (2019). Structural changes in the African
- 17 easterly jet and its role in mediating the effects of Saharan dust on the linear dynamics of
- 18 African easterly waves. *Journal of the Atmospheric Sciences*, 76(11), 3351-3365.
- 19 <https://doi.org/10.1175/JAS-D-19-0104.1>

- 20 Grogan, D. F. P., Lu, C.-H., Wei, S.-W., and Chen, S.-P., 2022. Investigating the impact
- 21 of Saharan dust aerosols on analyses and forecasts of African easterly waves by
- 22 constraining aerosol effects in radiance data assimilation, *Atmos. Chem. Phys.*, 22, 2385–
- 23 2398, <https://doi.org/10.5194/acp-22-2385-2022>.

- 24 Grotjahn, R., 2003. Baroclinic instability. *Encyclopedia of Atmospheric Sciences*, 419,
- 25 467.



- 1 Haarig, M., et al., 2019. Profiles of cloud condensation nuclei, dust mass concentration,
2 and ice-nucleating-particle-relevant aerosol properties in the saharan air layer over
3 barbados from polarization lidar and airborne in situ measurements. *Atmospheric*
4 *Chemistry and Physics*, 19(22):13773–13788.
- 5 Haywood, J. M., Pelon, J., Formenti, P., Bharmal, N., Brooks, M., Capes, G., ... & Tulet,
6 P. (2008). Overview of the dust and biomass-burning experiment and African monsoon
7 multidisciplinary analysis special observing period-0. *Journal of Geophysical Research:*
8 *Atmospheres*, 113(D23). <https://doi.org/10.1029/2008JD010077>
- 9 Hinkelman, L. M., 2019. The Global Radiative Energy Budget in MERRA and MERRA-
10 2: Evaluation with Respect to CERES EBAF Data, *Journal of Climate*, 32(6), 1973-1994,
11 <https://doi.org/10.1175/JCLI-D-18-0445.1>
- 12 Hopsch, S. B., C. D. Thorncroft, K. Hodge, and A. Aiyyer, 2007. West African storm
13 tracks and their relationship to Atlantic tropical cyclones. *J. Climate*, 20, 2468–2483.
- 14 Hoskins, B. J., James, I. N., & White, G. H. 1983. The Shape, Propagation and Mean-
15 Flow Interaction of Large-Scale Weather Systems, *Journal of Atmospheric*
16 *Sciences*, 40(7), 1595-1612, [https://doi.org/10.1175/1520-](https://doi.org/10.1175/1520-0469(1983)040%3C1595:TSPAMF%3E2.0.CO;2)
17 [0469\(1983\)040%3C1595:TSPAMF%3E2.0.CO;2](https://doi.org/10.1175/1520-0469(1983)040%3C1595:TSPAMF%3E2.0.CO;2)
- 18 Hosseinpour F., and E. M. Wilcox, 2014. Aerosol interactions with African/Atlantic
19 climate dynamics. *Env. Res. Let.*, 9, 075004, DOI: 10.1088/1748-9326/9/7/075004.
- 20 Hsieh J. S., K. H. Cook, 2005. Generation of African Easterly Wave Disturbances:
21 Relationship to the African Easterly Jet, *Mon. Wea. Rev.*, 133, 1311–1327,
22 <https://doi.org/10.1175/MWR2916.1>
- 23 Hsieh, J., & Cook, K. H. 2007. A Study of the Energetics of African Easterly Waves
24 Using a Regional Climate Model, *Journal of the Atmospheric Sciences*, 64(2), 421-440,
25 <https://doi.org/10.1175/JAS3851.1>



- 1 Hsu, N. C., Lee, J., Sayer, A. M., Kim, W., Bettenhausen, C., & Tsay, S. C. (2019).
- 2 VIIRS Deep Blue aerosol products over land: Extending the EOS long-term aerosol data
- 3 records. *Journal of Geophysical Research: Atmospheres*, 124(7), 4026-4053.
- 4 <https://doi.org/10.1029/2018JD029688>

- 5 Jones C, N. Mahowald, and C. Luo, 2003. The role of easterly waves on African Desert
- 6 dust transport. *J. Climate*, 16, 3617–3628, DOI: 10.1175/1520-
- 7 0442(2003)016<3617:troewo>2.0.co;2.

- 8 Jones C, N. Mahowald, and C. Luo, 2004. Observational evidence of African Desert dust
- 9 intensification of easterly waves. *Geophys. Res. Lett.*, 31, L17208, DOI:
- 10 10.1029/2004gl020107.

- 11 Kiladis G. N., C. D. Thorncroft, and N. M. J. Hall, 2006. Three-dimensional structure and
- 12 dynamics of African easterly waves part I: Observations. *J. Atmos. Sci.*, 63, 2212–2230,
- 13 <https://doi.org/10.1175/JAS3741.1>

- 14 Kim K. M., W. K. M. Lau, Y. C. Sud, and G. K. Walker, 2010. Influence of Aerosol-
- 15 Radiative forcing on the diurnal and seasonal cycles of rainfall over West Africa and
- 16 eastern Atlantic Ocean using GCM simulations. *Clim. Dyn. J.*, 35, 115–126,
- 17 10.1007/s00382-010-0750-1.

- 18 Konare, A., Zakey, A. S., Solmon, F., Giorgi, F., Rauscher, S., Ibrah, S., & Bi, X. J. J. O.
- 19 G. R. A. (2008). A regional climate modeling study of the effect of desert dust on the
- 20 West African monsoon. *Journal of Geophysical Research: Atmospheres*, 113(D12).
- 21 <https://doi.org/10.1029/2007JD009322>

- 22 Lau, K. M., and Kim, K. M., 2007. Cooling of the Atlantic by Saharan dust, *Geophys.*
- 23 *Res. Lett.*, 34, L23811, doi:10.1029/2007GL031538.

- 24 Lau K. M., K. M. Kim, Y. C. Sud, and G. K. Walker, 2009. A GCM study of the
- 25 response of the atmospheric water cycle of West Africa and the Atlantic to Saharan dust



- 1 radiative forcing *Ann. Geophys.*, 27, 4023–4037, <https://doi.org/10.5194/angeo-27-4023->
2 2009.
- 3 Lorenz E. N., 1955. Available potential energy and the maintenance of the general
4 circulation. *Tellus.*, 7, 157–167, <https://doi.org/10.1111/j.2153-3490.1955.tb01148.x>.
- 5 Liang, J., Chen, Y., Arellano, A. F., & Mamun, A. A., 2021. Model sensitivity study of
6 the direct radiative impact of saharan dust on the early stage of hurricane
7 earl. *Atmosphere*, 12(9), 1181.
- 8 Liu, D., Wang, Z., Liu, Z., Winker, D., and Trepte, C., 2008. A height resolved global
9 view of dust aerosols from the first year CALIPSO lidar measurements, *J. Geophys.*
10 *Res.*, 113, D16214, doi:10.1029/2007JD009776.
- 11 Ma P. L., K. Zhang, J. J. Shi, T. Matsui, A. Arking, 2012. Direct radiative effect of
12 mineral dust on the development of African easterly waves in late summer 2003–07. *J.*
13 *Applied Meteorology and Climate*, 51, 2090–2104, <https://doi.org/10.1175/JAMC-D-11->
14 0215.1.
- 15 Matsuki, A., Quennehen, B., Schwarzenboeck, A., Crumeyrolle, S., Venzac, H., Laj, P.,
16 and Gomes, L.: Temporal and vertical variations of aerosol physical and chemical
17 properties over West Africa: AMMA aircraft campaign in summer 2006, *Atmos. Chem.*
18 *Phys.*, 10, 8437–8451, <https://doi.org/10.5194/acp-10-8437-2010>, 2010.
- 19 Mamun, A., Chen, Y., & Liang, J., 2021. Radiative and cloud microphysical effects of
20 the Saharan dust simulated by the WRF-Chem model. *Journal of Atmospheric and Solar-*
21 *Terrestrial Physics*, 219, 105646
- 22 Mekonnen, A., Thorncroft, C. D., & Aiyyer, A. R., 2006. Analysis of Convection and Its
23 Association with African Easterly Waves, *Journal of Climate*, 19(20), 5405-5421,
24 <https://doi.org/10.1175/JCLI3920.1>
- 25 Meloni, D., di Sarra, A., Brogniez, G., Denjean, C., De Silvestri, L., Di Iorio, T.,
26 Formenti, P., Gómez-Amo, J. L., Gröbner, J., Kouremeti, N., Liuzzi, G., Mallet, M.,



- 1 Pace, G., and Sferlazzo, D. M. (2018). Determining the infrared radiative effects of
2 Saharan dust: a radiative transfer modelling study based on vertically resolved
3 measurements at Lampedusa, *Atmos. Chem. Phys.*, 18, 4377–4401,
4 <https://doi.org/10.5194/acp-18-4377-2018>
- 5 Ming Y., and V. Ramaswamy, 2011. A model investigation of aerosol-induced changes
6 in tropical circulation. *J. Climate*, 24, 5125–5133,
7 <https://doi.org/10.1175/2011JCLI4108.1>.
- 8 Myhre, G., et al., 2004. Intercomparison of satellite retrieved aerosol optical depth over
9 the ocean, *J. Atmos. Sci.*, 61, 499–513.
- 10 Nitta, T., and Y. Takayabu, 1985. Global analysis of the lower tropospheric disturbances
11 in the tropics during the northern summer of FGGE year. Part II: Regional characteristics
12 of the disturbances. *Pure Appl. Geophys.*, 123, 272–292
- 13 Norquist, D. C., E. Recker, and R. J. Reed, 1977. The energetics of African wave
14 disturbances as observed during the phase III of GATE. *Mon. Weather Rev.*, 105, 334–
15 342, [https://doi.org/10.1175/1520-0493\(1977\)105<0334:TEOAWD>2.0.CO;2](https://doi.org/10.1175/1520-0493(1977)105<0334:TEOAWD>2.0.CO;2).
- 16 Orlanski I., and J. Katzfey, 1991. The life cycle of a cyclone wave in the Southern
17 Hemisphere. Part I: Eddy energy budget. *J. Atmos. Sci.*, 48, 1972–1998,
18 [https://doi.org/10.1175/1520-0469\(1991\)048<1972:TLCOAC>2.0.CO;2](https://doi.org/10.1175/1520-0469(1991)048<1972:TLCOAC>2.0.CO;2).
- 19 Pasch, R. J., & Avila, L. A., 1994. Atlantic Tropical Systems of 1992, *Monthly Weather*
20 *Review*, 122(3), 539-548, [https://doi.org/10.1175/1520-](https://doi.org/10.1175/1520-0493(1994)122<0539:ATSO>2.0.CO;2)
21 [0493\(1994\)122<0539:ATSO>2.0.CO;2](https://doi.org/10.1175/1520-0493(1994)122<0539:ATSO>2.0.CO;2)
- 22 Perry, K. D., T. A. Cahill, R. A. Eldred, D. D. Dutcher, and T. E. Gill, 1997. Long-range
23 transport of North African dust to the eastern United States, *J. Geophys.*
24 *Res.*, 102, 11,225–11,238, doi.org/10.1029/97JD00260



- 1 Platnick, S., 2015. MODIS Atmosphere L3 Daily Product. NASA MODIS Adaptive
- 2 Processing System, Goddard Space Flight Center, USA:
- 3 http://dx.doi.org/10.5067/MODIS/MOD08_D3.061

- 4 Plumb, R. A., 1983. A new look at the energy cycle. *J. Atmos. Sci.*, 40, 1669–1688,
- 5 [https://doi.org/10.1175/1520-0469\(1983\)040<1669:ANLATE>2.0.CO;2](https://doi.org/10.1175/1520-0469(1983)040<1669:ANLATE>2.0.CO;2).

- 6 Prospero, J.M. and Lamb, P.J., 2003. African Droughts and Dust Transport to the
- 7 Caribbean: Climate Change Implications. *Science*, 302, 1024-1027.
- 8 <http://doi.org/10.1126/science.1089915>

- 9 Pytharoulis, I., & Thorncroft, C., 1999. The low-level structure of African easterly waves
- 10 in 1995. *Monthly Weather Review*, 127(10), 2266-2280.

- 11 Ramo, R., Roteta, E., Bistinas, I., Van Wees, D., Bastarrika, A., Chuvieco, E. and Van
- 12 der Werf, G.R., 2021. African burned area and fire carbon emissions are strongly
- 13 impacted by small fires undetected by coarse resolution satellite data. *Proceedings of the*
- 14 *National Academy of Sciences*, 118(9), p.e2011160118,
- 15 <https://doi.org/10.1073/pnas.2011160118>

- 16 Randles, C. A., et al., 2017. The MERRA-2 Aerosol Reanalysis, 1980 Onward. Part I:
- 17 System Description and Data Assimilation Evaluation, *Journal of Climate*, 30(17), 6823-
- 18 6850, <https://doi.org/10.1175/JCLI-D-16-0609.1>

- 19 Reale, O., Achuthavari, D., Fuentes, M., Putman, W. M., & Partyka, G., 2017. Tropical
- 20 Cyclones in the 7-km NASA Global Nature Run for Use in Observing System Simulation
- 21 Experiments, *Journal of Atmospheric and Oceanic Technology*, 34(1), 73-100,
- 22 <https://doi.org/10.1175/JTECH-D-16-0094.1>

- 23 Redemann, J., Wood, R., Zuidema, P., Doherty, S. J., Luna, B., LeBlanc, S. E., ... & Gao,
- 24 L. (2021). An overview of the ORACLES (ObseRvations of Aerosols above CLouds and
- 25 their intERactionS) project: aerosol–cloud–radiation interactions in the southeast Atlantic



- 1 basin. *Atmospheric Chemistry and Physics*, 21(3), 1507-1563.
- 2 <https://doi.org/10.5194/acp-21-1507-2021>
- 3 Reed R. J., A. Hollingsworth, W. A. Heckley, and F. Delsol, 1988. An evaluation of the
4 performance of the ECMWF operational system in analyzing and forecasting easterly
5 wave disturbances 15 SEPTEMBER 2013 W U E T A L . 6773 over Africa and the
6 tropical Atlantic. *Mon. Wea. Rev.*, 116, 824–865.
- 7 Remer, L. A., Levy, R. C., Mattoo, S., Tanré, D., Gupta, P., Shi, Y., ... & Holben, B. N.
8 (2020). The dark target algorithm for observing the global aerosol system: Past, present,
9 and future. *Remote sensing*, 12(18), 2900. <https://doi.org/10.3390/rs12182900>.
- 10 Rienecker, M. M., et al., 2008. The GEOS-5 Data Assimilation System—Documentation
11 of versions 5.0.1 and 5.1.0, and 5.2.0. NASA Tech. Rep. Series on Global Modeling and
12 Data Assimilation, NASA/TM-2008-104606, Vol. 27, 92 pp.
- 13 Rienecker M., et al., 2011. MERRA: NASA’s Modern-Era retrospective analysis for
14 research and applications. *J. Climate*, 24, 3624–3648, [https://doi.org/10.1175/JCLI-D-11-](https://doi.org/10.1175/JCLI-D-11-00015.1)
15 00015.1.
- 16 Roundy P. E., and W. M. Frank, 2004. A climatology of waves in the equatorial region. *J.*
17 *atmos. sci.*, 61, 2105–2032, [https://doi.org/10.1175/1520-](https://doi.org/10.1175/1520-0469(2004)061<2105:ACOWIT>2.0.CO;2)
18 0469(2004)061<2105:ACOWIT>2.0.CO;2.
- 19 Russell, J. O., Aiyyer, A., & Dylan White, J., 2020. African Easterly Wave Dynamics in
20 Convection-Permitting Simulations: Rotational Stratiform Instability as a Conceptual
21 Model. *Journal of Advances in Modeling Earth Systems*, 12(1), e2019MS001706.
- 22 Saidou Chaibou, A. A., Ma, X., & Sha, T. (2020). Dust radiative forcing and its impact
23 on surface energy budget over West Africa. *Scientific reports*, 10(1), 12236.
24 <https://doi.org/10.1038/s41598-020-69223-4>
- 25 Sayer, A. M., Hsu, N. C., Lee, J., Kim, W. V., & Dutcher, S. T. (2019). Validation,
26 stability, and consistency of MODIS Collection 6.1 and VIIRS Version 1 Deep Blue



- 1 aerosol data over land. *Journal of Geophysical Research: Atmospheres*, 124(8), 4658-
2 4688. <https://doi.org/10.1029/2018JD029598>
- 3 Soupiona, O., Papayannis, A., Kokkalis, P., Foskinis, R., Sánchez Hernández, G., Ortiz-
4 Amezcua, P., Mylonaki, M., Papanikolaou, C.-A., Papagiannopoulos, N., Samaras, S.,
5 Groß, S., Mamouri, R.-E., Alados-Arboledas, L., Amodeo, A., and Psiloglou, B.:
6 EARLINET observations of Saharan dust intrusions over the northern Mediterranean
7 region (2014–2017): properties and impact on radiative forcing, *Atmos. Chem. Phys.*, 20,
8 15147–15166, <https://doi.org/10.5194/acp-20-15147-2020>, 2020.
- 9 Thorncroft, C. D. and K. Hodges, 2001. African Easterly Wave Variability and Its
10 Relationship to Atlantic Tropical Cyclone Activity. *J. Climate*, 14, 116-1179.
- 11 Thorncroft C. D., N. M. Hall, G. N. Kiladis, 2008. Three-dimensional structure and
12 dynamics of African easterly waves. Part III: genesis. *J. Atmos. Sci.*, 65, 3596–607,
13 <https://doi.org/10.1175/2008JAS2575.1>.
- 14 Weinzierl, B., et al., 2017. The saharan aerosol long-range transport and aerosol–cloud-
15 interaction experiment: Overview and selected highlights. *Bulletin of the American*
16 *Meteorological Society*, 98(7):1427 – 1451.
- 17 Wilcox E. M., W. K.M. Lau, and K. M. Kim, 2010. A Northward shift of the North
18 Atlantic Ocean intertropical convergence zone in response to summertime Saharan dust
19 outbreaks. *Geophys. Res. Lett.*, 37, L04804, DOI:10.1029/2009GL041774.
- 20 Wright, J. S., Sun, X., Konopka, P., Krüger, K., Legras, B., Molod, A. M., Tegtmeier, S.,
21 Zhang, G. J., and Zhao, X., 2020. Differences in tropical high clouds among reanalyses:
22 origins and radiative impacts, *Atmos. Chem. Phys.*, 20, 8989–9030,
23 <https://doi.org/10.5194/acp-20-8989-2020>.
- 24 Wu, M.L.C., Reale, O. and Schubert, S.D., 2013. A characterization of African easterly
25 waves on 2.5–6-day and 6–9-day time scales. *J. Clim.*, 26(18), pp.6750-6774.



- 1 Zhao, L., X. Lee, and S. Liu, 2013. Correcting surface solar radiation of two data
- 2 assimilation systems against FLUXNET observations in North America, *J. Geophys. Res.*
- 3 *Atmos.*, 118, 9552–9564, doi:10.1002/jgrd.50697.
- 4 Zuidema, P., Redemann, J., Haywood, J., Wood, R., Piketh, S., Hipondoka, M., and
- 5 Formenti, P.: Smoke and clouds above the southeast Atlantic: Upcoming field campaigns
- 6 probe absorbing aerosol's impact on climate, *B. Am. Meteorol. Soc.*, 97, 1131–
- 7 1135, <https://doi.org/10.1175/BAMS-D-15-00082.1>, 2016.

8

9 **Table 1** MODIS and MERRA-2 data information applied in this study

Dataset	Product Name	Variables	Spatial Resolution	Temporal Resolution	Data Reference
MODIS	MOD08_D3	550-nm AOD, Deep-blue AOD	1°×1°	daily	Platnick (2015)
MERRA-2	M2I6NPANA	U, V, T, H	0.5°×0.625°	3-hourly (averaged to daily)	GMAO (2015a)
	M2T1NXRAD	SWF _{TOA_{tot}} , SWF _{TOA_{clean}} , SWF _{sfc_{tot}} , SWF _{sfc_{clean}}	0.5°×0.625°	1-hourly (averaged to daily)	GMAO (2015b)
	M2I3NPASM	Omega	0.5°×0.625°	3-hourly (averaged to daily)	GMAO (2015c)

10

11 **Table 2** The coordinates of domains of transient changes across the tropical Atlantic

12 Ocean:

AEW domains		
Description	Central Atlantic	Eastern Atlantic



Northern track waves	18° to 24°N -45° to -30°E	18° to 24°N -30° to -15°E
Downstream of jet-axis	12° to 18°N -45° to -30°E	12° to 18°N -30° to -15°E
Southern track waves	6° to 12°N -45° to -30°E	6° to 12°N -30° to -15°E

1

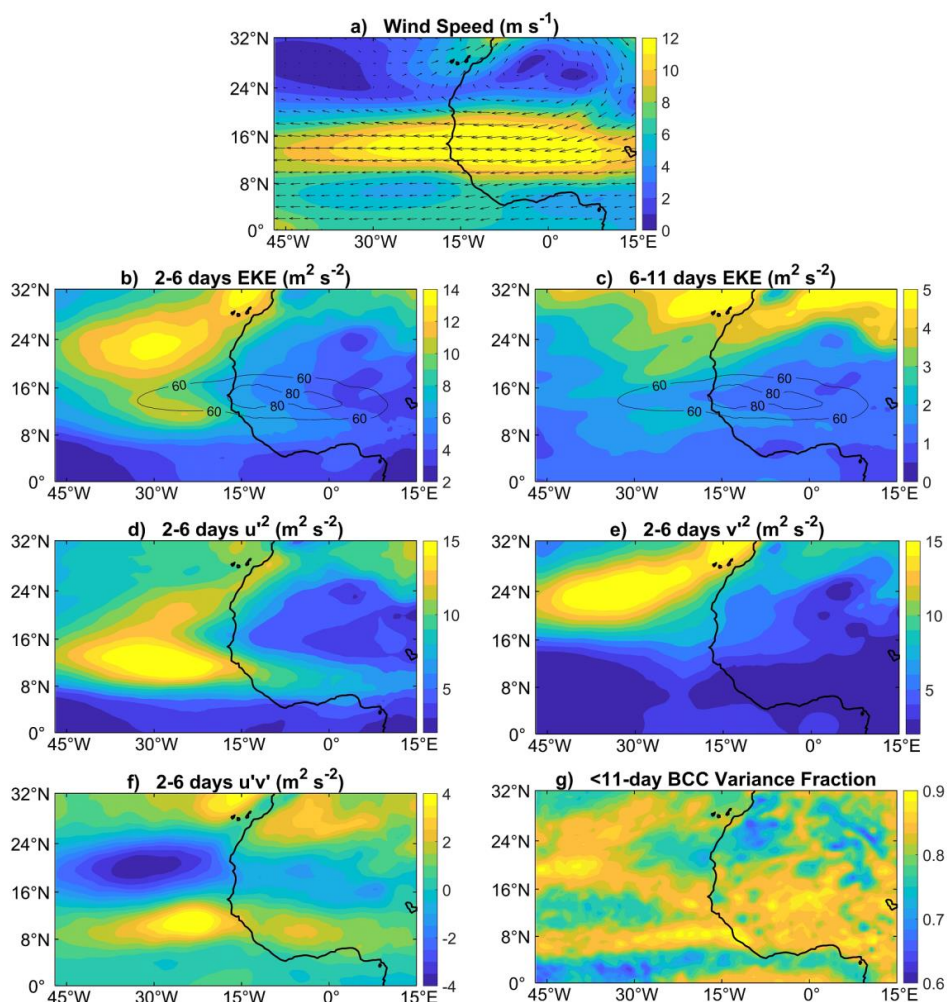
2

3 **Table 3** Summary of lag analyses showing AEWs evolution before and after dust peaks in

4 OSAL:

Downstream development of eddy activity – Central Atlantic			
	Before Dust-peak	Simultaneously at Dust-peak	After Dust-peak
Northern track AEWs	T < 0 Negligible changes in EKE	T = 0 EKE starts increasing	T = +3 Max EKE
Along the AEJ axis	T < 0 Negligible changes in EKE	T = 0 Decrease of EKE	T = +2 EKE starts increasing T ~ +3 to +4 Max EKE
Southern track AEWs	T = -3 EKE starts increasing	T = 0 Increase of EKE	T = +2 Max EKE

5

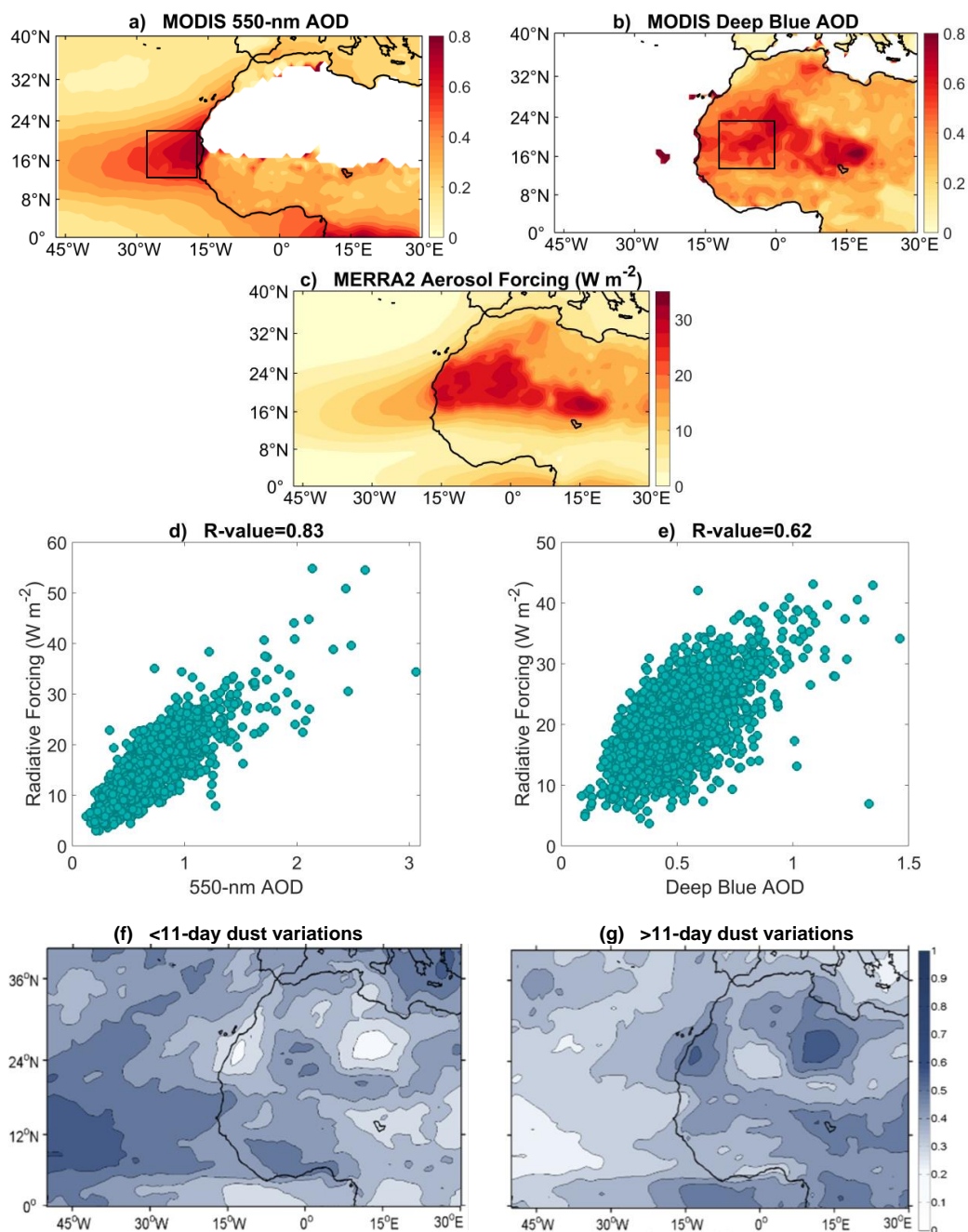


1

2 **Figure 1** (a) Long-term mean of 600-hPa wind speed (ms^{-1}) from MERRA-2 reanalysis over JJA,
3 2000-2021. (b) Same as (a) but for 2-6-day bandpass filtered EKE (m^2s^{-2}) at 600-hPa. (c) Same as (b) but for
4 6-11-day bandpass filtered EKE. (d) Same as (b) but shows the 2-6-day variance of zonal wind, $\overline{u'^2}$, (m^2s^{-2}).
5 (e) Same as (b) but shows the 2-6-day variance of meridional wind, $\overline{v'^2}$, (m^2s^{-2}). (f) Same as (b) but for the
6 2-6-day filtered transient momentum fluxes, $\overline{u'v'}$, (m^2s^{-2}). (g) Fraction of less than the 11-day variance of
7 600-hPa Baroclinic Conversion (BCC) with respect to the total variance of BCC in JJA, 2000-2021.

8

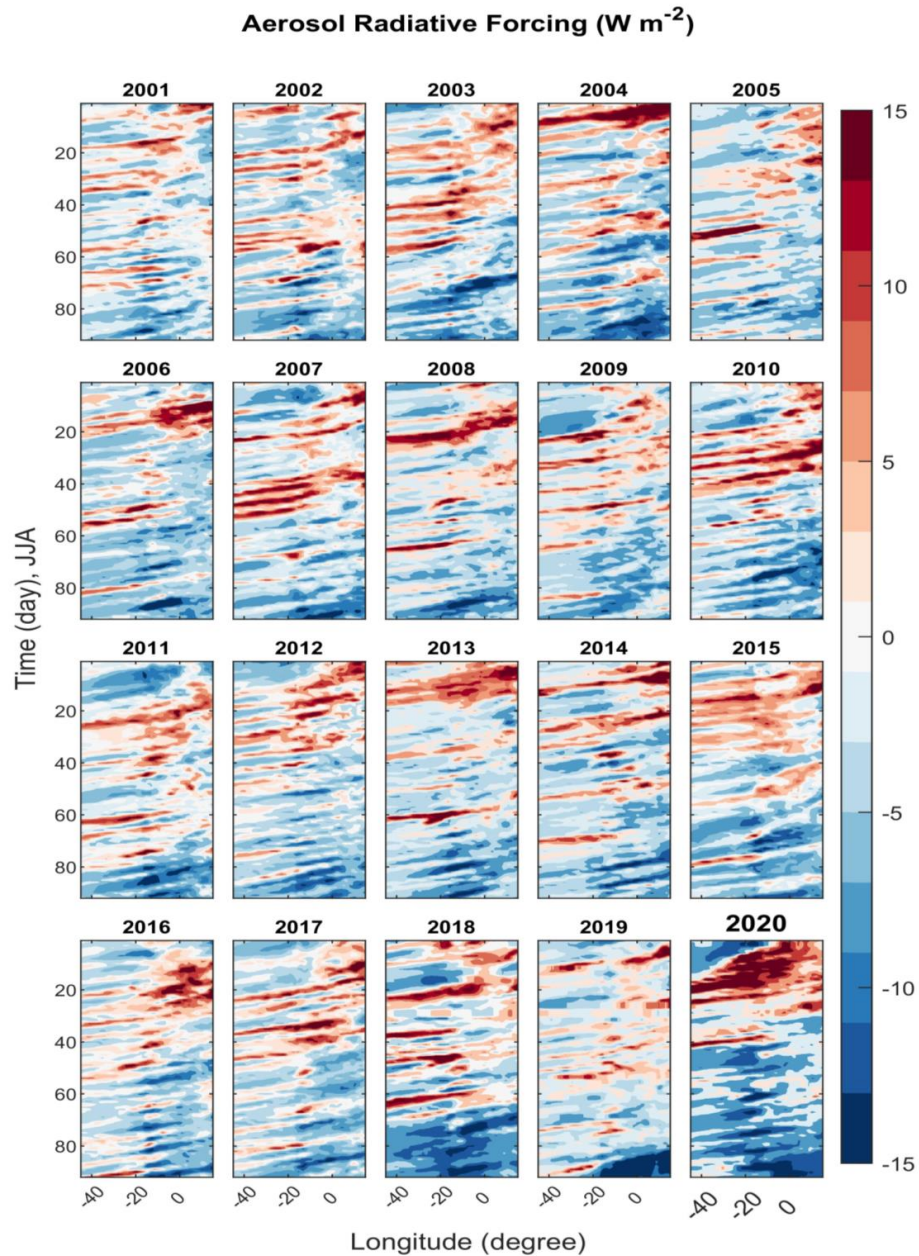
9



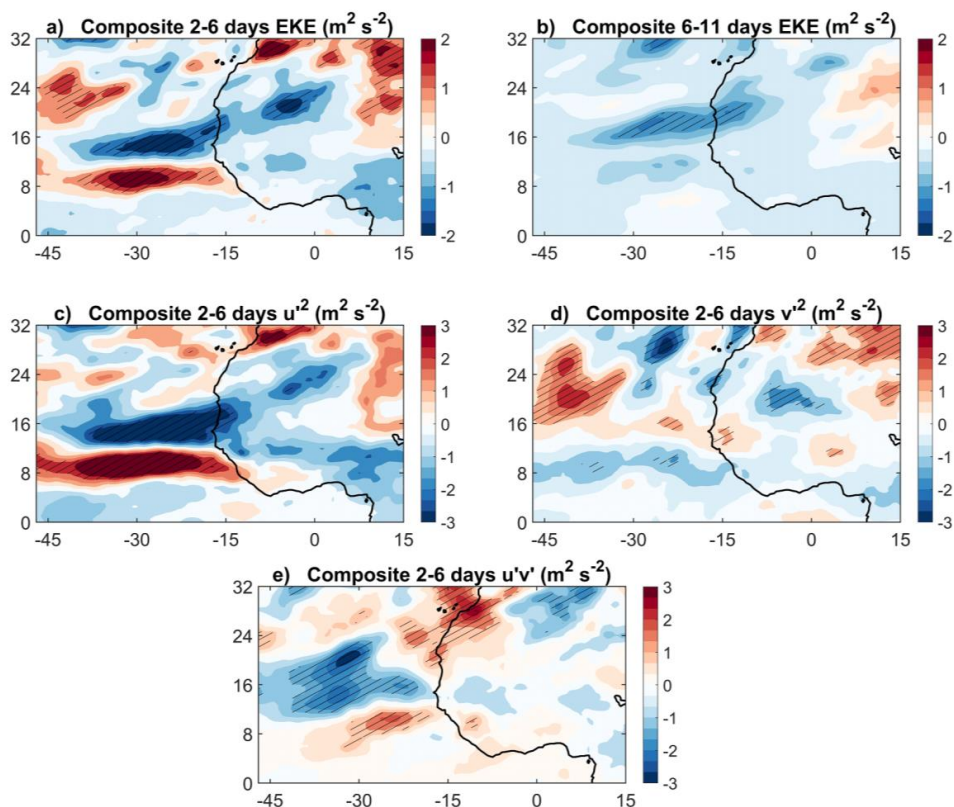
1
2 **Figure 2** (a) Long-term mean of 550-nm aerosol optical depth (AOD) from the MODIS over JJA, 2000-
3 2021. (b) Same as (a) but for 470-nm MODIS deep-blue AOD. (c) Same as (a) but for aerosol shortwave
4 radiative forcing (Wm^{-2}) in the atmosphere (TOA minus surface) from the MERRA-2 reanalysis. (d)



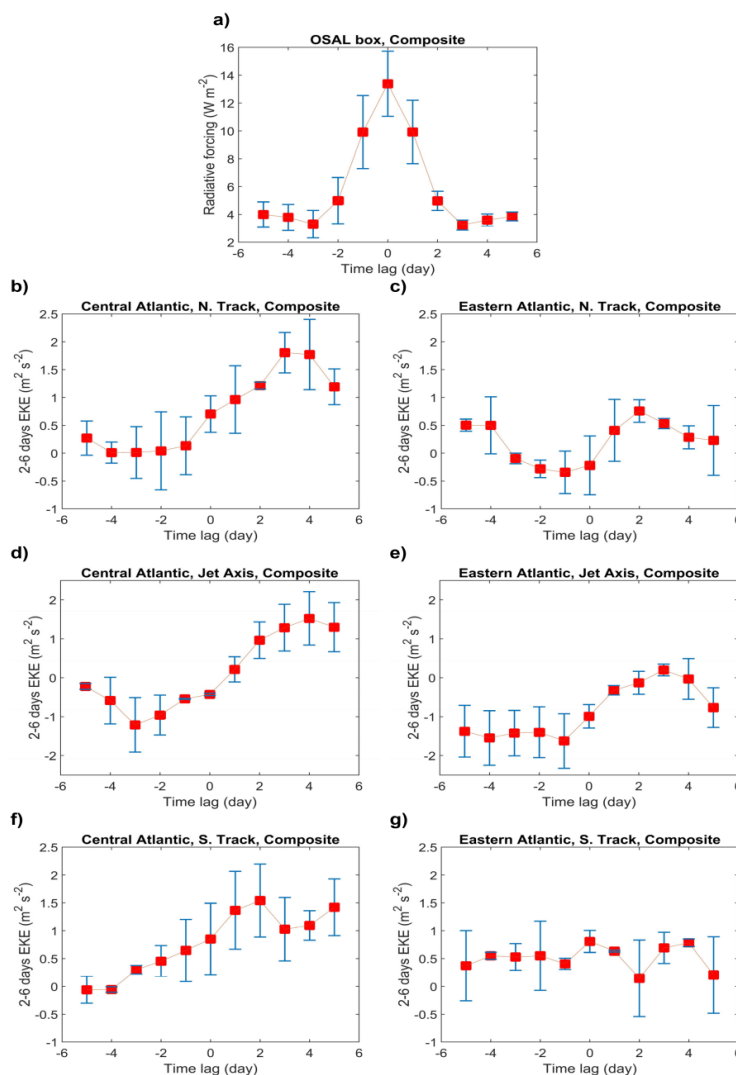
1 Relationship between MODIS AOD and MERRA-2 radiative forcing for JJA, 2000-2021. Each data point
2 shows daily data averaged over the OSAL region (rectangle in 2a). The results are statistically significant
3 with P-value < 0.05. (e) Same as (d), but for MODIS deep blue AOD over the land (rectangle in 1b). (f)
4 Fraction of variations of less than 11-day for the variance of aerosol radiative forcing with respect to the total
5 variance using the long-term mean of aerosol radiative forcing in the atmosphere (TOA minus surface) from
6 the MERRA-2 reanalysis over JJA, 2000-2021. (g) Same as (f) but for variations of more than 11-day.
7



1
2 **Figure 3** Time-longitude Hovmöller diagrams of aerosol radiative forcing daily anomalies (Wm^{-2}) using the
3 MERRA-2 reanalysis for all individual boreal summer seasons, JJA from 2000 to 2021, meridionally
4 averaged ($12\text{--}22^\circ \text{N}$) over the OSAL domain (rectangle in Figure 2a). Daily anomalies of aerosol radiative
5 forcing are calculated with respect to the seasonal time average of radiative forcing for each year.



1
2 **Figure 4** (a) Composite 600-hPa 2-6-day filtered EKE (m^2s^{-2}) values for the times corresponding to the upper
3 quartile aerosol radiative forcing minus the EKE values of the times corresponding to the lower quartile
4 aerosol radiative forcing over the OSAL domain (rectangle in Figure 2a). The calculations are conducted
5 using the MERRA-2 reanalysis for JJA, 2000-2021. (b) Same as (a) but for 6-11-day filtered EKE (m^2s^{-2}).
6 (c) same as (a) but for the 2-6-day variance of zonal wind, $\overline{u'^2}$, (m^2s^{-2}). (d) As in (a) but for 2-6-day the
7 variance of meridional wind, $\overline{v'^2}$, (m^2s^{-2}). (e) Same as (a) but for the 2-6-day filtered momentum fluxes, $\overline{u'v'}$,
8 (m^2s^{-2}).



1

2 **Figure 5** (a) Daily time series of composite aerosol radiative forcing for the days in the upper quartile
 3 minus those days in the lower quartile radiative forcing, spatially averaged over the OSAL domain
 4 (rectangle in Figure 2a). T = 0 is assigned for the days with the highest variability of aerosol radiative
 5 forcing in the OSAL. T = +/- 1, T = +/- 2, T = +/- 3, T = +/- 4, and T = +/- 5 are assigned for five days
 6 before and five days after of each individual dust event, averaged over for 22 years, JJA, 2000-2021. (b)
 7 Same as (a) but for the composite 2-6 day filtered EKE at 600-hPa, spatially averaged over the northern
 8 track AEWs in the central Atlantic (18° to 24°N, -45° to -30°E). (c) Same as (b) but for the eastern Atlantic
 9 (18° to 24°N, -30° to -15°E). (d) Same as (b) but spatially averaged over the domain, downstream of the
 10 AEJ in the central Atlantic (12° to 18°N, -45° to -30°E). (e) same as (d) but for the eastern Atlantic (12° to
 11 18°N, -30° to -15°E). (f) same as (b) but spatially averaged over the southern track of the AEWs in the
 12 central Atlantic (6° to 12°N, -45° to -30°E). (g) Same as (f) but for the eastern Atlantic (6° to 12°N, -30° to
 13 -15°E). The domains of the wave activity are listed in Table 3.